

Communication

Crystalline Flat Surface Recovered by High-Temperature Annealing after Laser Ablation

Daniel Smith ¹, Soon Hock Ng ^{1,*}, Amanda Tang ¹, Tomas Katkus ¹, Daniel Moraru ² and Saulius Juodkazis ^{1,3,*}

¹ Optical Sciences Centre (OSC) and ARC Training Centre in Surface Engineering for Advanced Materials (SEAM), School of Science, Computing and Engineering Technologies, Swinburne University of Technology, Hawthorn, VIC 3122, Australia; danielsmith@swin.edu.au (D.S.); 101739224@student.swin.edu.au (A.T.); tkatkus@swin.edu.au (T.K.)

² Research Institute of Electronics, Shizuoka University, Johoku 3-5-1, Hamamatsu 432-8011, Japan; moraru.daniel@shizuoka.ac.jp

³ World Research Hub Initiative (WRHI), School of Materials and Chemical Technology, Tokyo Institute of Technology, 2-12-1, Ookayama, Meguro-ku, Tokyo 152-8550, Japan

* Correspondence: soonhockng@swin.edu.au (S.H.N.); sjuodkazis@swin.edu.au (S.J.)

Abstract: Ultra-short laser pulses (1030 nm/230 fs) were used to laser ablate the surface of crystalline sapphire (Al₂O₃) at high intensity per pulse 20–200 TW/cm²/pulse. Laser-ablated patterns were annealed at a high temperature of 1500 °C. Surface reconstruction took place, removing the ablation debris field at the edges of ablated pits in oxygen flow (O₂ flow). Partial reconstruction of ripples was also observed when multi-pulse ablated surfaces were annealed at high temperature in O₂ flow. Back-side ablation of a 0.5-mm-thick Al₂O₃ produced high surface roughness ~1 μm which was reduced to ~0.2 μm by high-temperature annealing at 1500 °C for 2 h in O₂. Improvement of surface quality was due to restructuring of the crystalline surface and sublimation, while the defined 3D shape of a micro-lens was not altered after HTA (no thermal morphing).

Keywords: ablation; light–matter interaction; femtosecond lasers; nanoscale; high-temperature annealing



Citation: Smith, D.; Ng, S.H.; Tang, A.; Katkus, T.; Moraru, D.; Juodkazis, S. Crystalline Flat Surface Recovered by High-Temperature Annealing after Laser Ablation. *Photonics* **2023**, *10*, 594. <https://doi.org/10.3390/photonics10050594>

Received: 24 March 2023

Revised: 14 May 2023

Accepted: 15 May 2023

Published: 19 May 2023



Copyright: © 2023 by the authors. Licensee MDPI, Basel, Switzerland. This article is an open access article distributed under the terms and conditions of the Creative Commons Attribution (CC BY) license (<https://creativecommons.org/licenses/by/4.0/>).

1. Introduction: High Intensity > TW/cm² Crystal Processing

Matter at extreme conditions of pressures above 1 megabar (10¹¹ Pa) and high temperatures as in the interior of planets—the warm dense matter (WDM)—is an active field of research [1]. High-pressure and high-temperature phases of materials can be created by ultra-fast thermal quenching of a small modified volume inside transparent material, e.g., sapphire [2,3]. Internally confined micro-explosions create WDM conditions similar to the centre of the Earth. For point-like energy deposition, it is informative to present Sedov's solution, where the radius, R , of the shock wave is increasing in time t as [4,5]:

$$R(t) = \left(\frac{E_p}{K(\gamma)\rho_0} \right)^{1/(2+i)} t^{2/(2+i)}, \quad (1)$$

where E_p is the instantaneous (in space and time) release of energy, $K(\gamma) = (0.6–0.8)$ is the constant dependent on the adiabatic coefficient $\gamma = C_p/C_v$ ($\gamma = 1.4$ for air), ρ_0 is the mass density in an unperturbed medium, and i is the dimensionality coefficient $i = 3$ for spherical and $i = 2$ for cylindrical explosion; here, $C_{p,v}$ is the heat capacities at constant pressure and volume, respectively. Such a shock wave launched from the focal volume creates highly dynamic conditions of high pressures and temperatures, which lead to formation of new materials [2,3]. In addition, metastable amorphous phases can be produced as shown for sapphire [6] due to ultra-fast thermal quenching of small volumes modified by fs-laser pulse-triggered explosions. Spatially confined, energy deposition of ~40 fs onto a water surface triggers shock waves inside the water and the surrounding air

which causes emissions of X-rays and THz [7]. This can be a single optical cycle ($\sim 1\text{--}3$ ps) due to the point-like energy deposition in time and space.

The micro-explosion hydrodynamics was shown to follow the established and tested macroscopic versions of strong explosions [8]. Evolution of the micro-explosion is characterized by the independent parameters: energy E (or pressure P), density ρ , and radius r , while the two other parameters required for the full description of the hydrodynamic processes, the velocity and time, can be expressed as $v = \sqrt{P/\rho} \equiv \sqrt{E/(r^3\rho)}$ and $t = r^{5/2}\sqrt{\rho/E}$, respectively. It is shown that micro-explosions triggered by tightly focused fs-laser pulses are self-similar with macro-explosions made by a 10^{21} large energy deposition when the time t and space r are 10^7 times larger [8]. All hydrodynamic phenomena with the same initial pressure and density but differing in space and time scales are described by the same hydrodynamic equations. In astrophysics, these same equations are used to describe the propagation of shock waves in self-gravitating perfect gases for isothermal flows [9], studying the dynamics of the envelope in supernova remnants [10,11], and the expansion of supernova shells [12].

Strong structural modifications induced by high-intensity ultra-short laser pulses could be modified by a post-processing steps of high temperature annealing (HTA) as recently demonstrated for micro-optical elements laser ablated out of crystalline sapphire Al_2O_3 [13]. HTA is a commonly used process for changing the surface morphology of different materials [14–17]. It has been used to make the particle size of high-temperature alloy thin films smaller [14], to create ceramic devices from polymers [17], and to smooth out germanium layers on silicon substrates [15] and terraces of chemically etched SrTiO_3 [16]. The roughness evolution of rapidly annealed surfaces is well understood; as the annealing time increases, the roughness decreases linearly [18]. Germanium, silicon, and some alloys have lower melting temperatures, making them easier to control. Sapphire, on the other hand, has a high melting temperature at 2053°C requiring more specialised equipment to reach these temperatures. In this study, it is shown that using temperatures between 1400°C to 1600°C and different gaseous environments, it is possible to alter the surface morphology of crystalline sapphire. In glasses, the softening point, at which a material does not become liquid as it would at the melting point but becomes malleable [19] is used; however, in crystals, only thermally activated surface diffusion on an atomic scale as well as sublimation is occurring. Sublimation is the process by which a solid material turns to gas without passing through the liquid phase. In crystals, sublimation causes them to create step-like structures, [20] as has been shown with $\text{GaN}(0001)$ [21], $\text{GaAs}(001)$ [22,23], and $\text{Si}(111)$ [24,25]. For each of these materials, both Monte Carlo simulation and experimental results showed agreement on the appearance of step-like structures and in the case of $\text{Si}(111)$, it was possible to nano-texture the surface with the sublimation method. The theory here is to balance the removal of material through the sublimation process with the growth of the crystalline structure to create the step surface. Sapphire sublimation has been used before on sapphire spheres 1 mm in diameter with much longer annealing times of 7.5 h and 1.5 h and at temperatures of 1500°C and 1850°C , respectively, in H_2 gas [26]. The vaporisation temperature for Al_2O_3 at a pressure of 1 atmosphere ranges from 2114.35°C to 2249.35°C [27]. The advantage of HTA of crystals is the preservation of large micro-scale structures and patterns, while reconstruction and smoothing of laser-treated regions takes place at nanoscale.

Here, we show the results of laser ablation of sapphire (Al_2O_3) and its high-temperature annealing for surface roughness reduction and reconstruction of surfaces with ablated ripples. The conditions to recover a crystalline smooth surface up to the rim of the ablated pits were found, which can be useful for applications to 2D materials. It is shown that back-side ablation of Al_2O_3 in air which produced roughness of $\sim 1\ \mu\text{m}$ was reduced to $<200\ \text{nm}$ after HTA at 1500°C for 2 h.

2. Samples and Methods

2.1. Sapphire

The PHAROS (Light Conversion Ltd., Vilnius, Lithuania) laser system was used to irradiate the surface of the Al_2O_3 on the front and the back-side. The Al_2O_3 samples have ~ 0.5 mm thicknesses. Al_2O_3 is a hard and inert material that requires ~ 10 TW/cm² intensities for ablation at near-IR 800–1000 nm wavelengths where multi-photon absorption is required to seed an efficient avalanche generation of free electrons for a wide bandgap ~ 8 –9 eV dielectric [28]. Among its virtues is high transparency in UV-to-IR spectral range (200–4000 nm) and high heat conductivity. This makes sapphire optics a promising target for industrial and space applications.

2.2. Laser Ablation Conditions

The PHAROS (Light Conversion Ltd.) laser system with $\lambda = 1030$ nm wavelength, $t_p = 230$ fs pulse duration, focusing with objectives lenses with numerical apertures of $NA = 0.26$ and $NA = 0.14$, resulted in focal spots calculated by Airy disk formula $2r = 1.22\lambda/NA$ of ≈ 4.8 μm and ≈ 8.9 μm , respectively. The Rayleigh length is $z_R = \pi r^2/\lambda = 35.62$ μm and 122.6 μm , which is half of the depth of focus (in air). For example, for the pulse energy of $E_p = 1$ μJ (on the sample), fluence was $F_p = 5.45$ J/cm² and average intensity $I_p = 24$ TW/cm². Laser repetition rate was $f_r = 200$ kHz and linear density of pulses was varied for larger or smaller overlap (typically 10^2 – 10^3 pulses/mm), which affected the material removal rate. The laser writing velocity was up to 15 mm/s for a position sensitive output, which was important for the high-precision ablation of micro-lenses in a multi-pass scanning mode. In general, this is a 2D/3D sculpturing method that can reach sub-micron precision when it is performed in the light-induced back-side wet etching (LIBWE) mode [29]. Specific details of laser patterning, if different from those listed above, are shown where applicable.

2.3. High-Temperature Annealing

High-temperature annealing (HTA) was carried out using a tube furnace (Model RHTC, Nabeterhm, Germany). The recipe starts by ramping the temperature up to 1500 °C at 150 °C an hour. The next step is holding the temperature at 1500 °C for 2 hours and afterwards ramping down to 1400 °C at 200 °C per hour. The final step is cooling down to 30 °C at 100 °C for an hour to finish the procedure. The extra step down to 1400 °C before cooling to 30 °C is used as a test for the limits of the tube furnace. This may be important if rapid quenching is required for further experimentation on the lenses. Currently, rates of up to 500 °C per hour have been tested.

3. Results and Discussion

3.1. Roughness Reduction of Ablated Sapphire Surfaces

Front-side ablation was used with laser pulses traveling from air-into- Al_2O_3 ; back-side ablation occurs when the focus is placed onto the exit plane (Al_2O_3 -to-air). This is usually possible with samples thinner than 0.5 mm and at less tight focusing with $NA < 0.4$; see Section 3.3 for the back-side ablation and HTA. It took ~ 30 min to ablate the profile of a 1-mm-diameter lens (Figure 1a) with a height of $h = 15$ μm . The surface roughness of the aspherical ablated surface was $\sim 200 \pm 50$ nm and it was reduced to 70 ± 30 nm after 2 h annealing (Figure 1c). However, light scattering was still strong and the surface remained visibly white. Initial roughness was also dependent on the focusing conditions and pulse overlap during ablation. Other smoothing strategies need to be tested, e.g., ablation with more focused pulses. When ablation took place at the very top of the lens profile (surface of sapphire), there was a strong change in ablation conditions, which resulted in a non-ablated plateau, which is ≈ 150 μm in diameter (Figure 1). This is a known issue and can be circumvented by placing a micro-layer of a matching refractive index material, e.g., a silica film, that allows to ablate sapphire [30]; the added layer is later washed out in a solvent/acid.

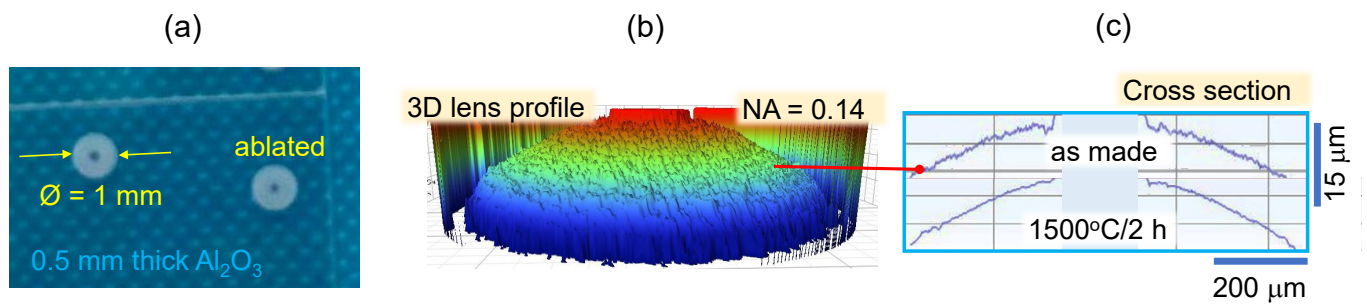


Figure 1. (a) A 1-mm-diameter lens ablated on sapphire Al₂O₃ c-plane with fs-laser pulses 1030 nm/230 fs. (b) 3D Bruker ContourGT Optical Profiler scan. (c) Roughness reduction by a high-temperature annealing (HTA) at 1500 °C for 2 h in N₂ flow of 200 mL/hour; same micro-lens. The center of the lens was not ablated for this front-side ablation mode due to a π -phase change of the reflected pulse. Ablation was made at a pulse density of 750 pulses/mm; NA = 0.14 (Mitutoyo). Linear polarisation of the E-field of laser pulses was horizontal. Pulse energy was $E_p = 4.375 \mu\text{J}$ (on sample). Fluence was $F_p = 6.91 \text{ J/cm}^2$.

The effect of HTA was examined through the ablation of crystalline flat c-plane Al₂O₃, which led to better understanding of surface changes. Since the maximum temperature used was 1500 °C, which is much lower than the melting point of Al₂O₃ ~2050 °C, surface restructuring by surface tension-driven flow of the molten phase was absent and other contributions from surface diffusion at atomic level, coarsening of debris nanoparticles, and sublimation took place. Sapphire has a melting point of 2053 °C and boiling temperature of 2980 °C. It has recently been shown that lower temperatures with larger times can also yield surface re-flow, which can be understood from length of diffusion scaling $\propto \sqrt{D_s \times t}$, where D_s [cm²/s] is the surface diffusion coefficient and t is time. Temperatures of 1100 °C and 1200 °C at 3, 6, 9, 18, and 30 h (in air ambience) have been tested and showed smoothing of c-plane sapphire terraces in step configurations [31]. Laser-modified regions under high-intensity irradiation in air might also have surface formation of ceramic ALON phase (AlN)_x·(Al₂O₃)_{1-x} with $x = 0.30\text{--}0.37$ or AlN [32]. When sapphire was placed in N₂ flow, the crystalline flat c-plane surface of Al₂O₃ changed to a nanotextured surface as shown by the SEM images in Figure A1a, and the entire piece of Al₂O₃ looks frosted and translucent as shown by the optical image in Figure A1b.

Generation of defects, vacancies, and interstitials under high intensity fs-pulses is taking place, e.g., F⁺ color center of the oxygen vacancy with a trapped electron created by fs-laser machining of sapphire is fully annealed at 1100° [33]. Frenkel pair defects interstitial—vacancy observed earlier by MeV-electron irradiated high-pressure cubic-BN was induced by fs-laser pulses [34] at similar conditions as used in this study. Chemical bond-breaking by high-intensity laser pulses can create metal-enriched regions on the surface of oxides and nitrides due to formation of volatile O₂ and N₂. Such laser-ablated surfaces of oxides rich with defects and debris and depleted of oxygen are expected to be restructured by HTA. We chose O₂ flow in order to facilitate surface migration of Al atoms to form terraces of Al₂O₃ under oxygen supply. This is one probable contribution to the formation of smooth crystalline surface.

3.2. Recovery of Crystalline Smooth Surface on Ablated Sapphire

When focusing using a less tight objective lens NA < 0.14 and carrying out single-pulse ablation with HTA in N₂ flow, there were more debris left after annealing as compared with samples annealed in O₂ (Figure 2). Nitrogen-rich atmosphere was not favorable to recovery of crystalline surface as compared with oxygen flow (see discussion above). Also, a pattern of single pulse ablation showed non-periodic structure with close-to-wavelength feature length. In addition, there was no typical ablation crater, rather a nano-textured surface resembling thermally quenched molten phase. The pulse fluence used was $F_p \approx 10 \text{ J/cm}^2$ or average intensity of $I_p \approx 43 \text{ TW/cm}^2$, which is smaller by more than an order of magni-

tude than the self-clamping intensity of fs-pulse $\sim 10^{14}$ W/cm² when multi-filaments are formed in air [35], and could cause a random pattern of dot-like modifications similar to those in the SEM image (Figure 2). Formation and quenching of a molten phase is more probable. Under such high intensity 43 TW/cm²/pulse exceeding the ablation threshold of sapphire by ~ 5 times, formation of a highly excited plasma skin layer of tens of nanometers was expected during the laser pulse [36]. Light-matter interaction takes place as if there is a nano-film of different optical permittivity $\epsilon \equiv \tilde{n}$ placed on dielectric sapphire; $\tilde{n} = n + i\kappa$ is the complex refractive index. Such transient material state described by changing permittivity $\epsilon(t)$ is called Die-Met (from dielectric and metal-like plasma) [36]. It has strong absorption due to reduced n and increased κ due to electron generation and is also referred to as epsilon-near-zero (ENZ) state $\epsilon = (n - \kappa)^2 + i2n\kappa$ [37].

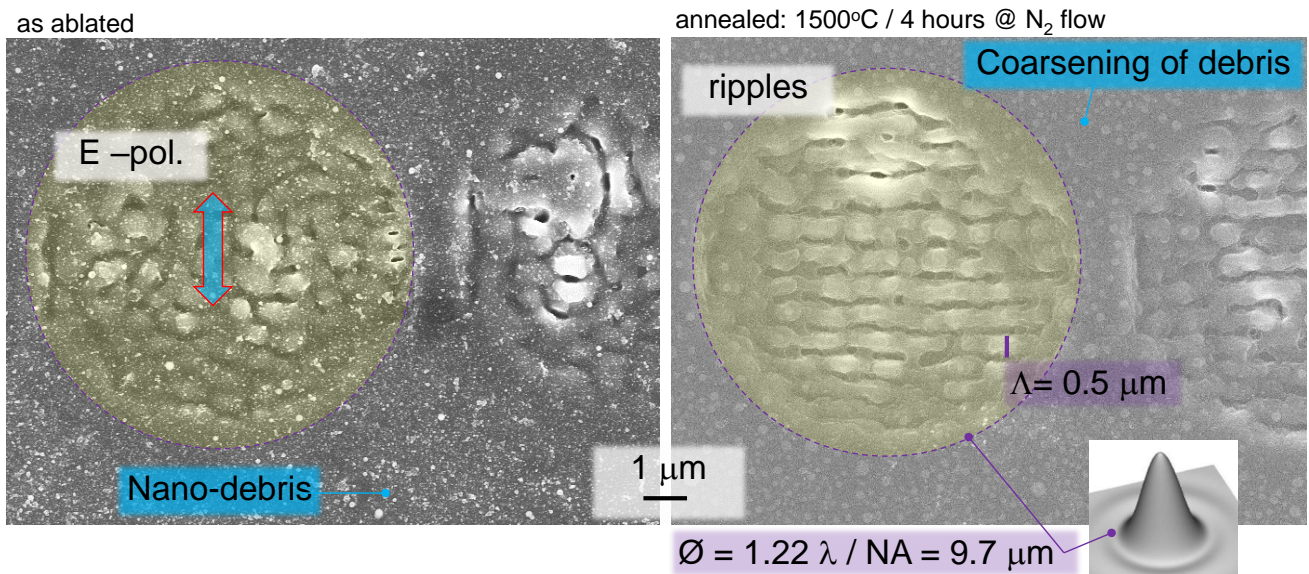


Figure 2. Single-pulse ablation and HTA of Sapphire (Al₂O₃) c-plane. HTA at 1500 °C for 2 h in N₂ flow. Ablation was made by one pulse per ablation site. Focusing of 1030 nm/230 fs pulses was carried out with an objective lens of numerical aperture $NA = 0.14$ (Mitutoyo). Linear polarisation of the E-field of laser pulses is shown by arrow marker. Pulse energy was $E_p = 6.25$ μJ (on sample). Fluence was $F_p = 9.87$ J/cm².

The ablation of thin films, which proceeds after the end of the laser pulse, follows an imprint of an fs-laser pulse intensity. Such modulation has $(\lambda/n)/2$ period and, under multi-pulse exposure, reveals itself as ripples [38]. After HTA, a more orderly ripple pattern emerged with period smaller than $\Lambda < \lambda$. The period of ripple-like pattern which evolved after HTA (Figure 2) resembles ripples ablated under multi-pulse exposure. We put forward here a conjecture (for future validation) that light intensity modulation $\sim \lambda/2$ occurred due to the presence of highly excited plasma nano-layer. Such modification of sub-surface region at the sapphire-plasma interface is hidden from SEM observation in Figure 2, which shows surface of a quenched molten phase. HTA was responsible for restructuring the surface and the imprinted modification was revealed. Figure 3 shows closeup SEM views of the ripples with evident re-crystallisation following c-plane of Al₂O₃ (hexagonal pits). Even though HTA temperature protocol was the same, the surface quality of HTA-treated ablated surface had more debris as compared with that made under O₂ flow (Figure 4).

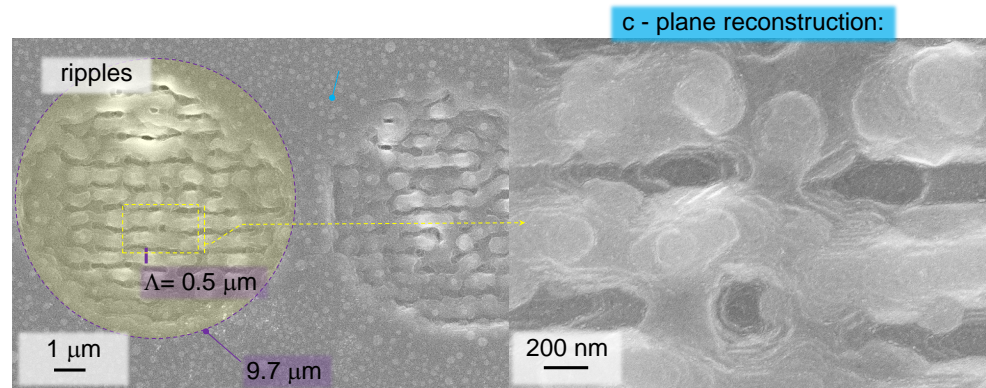


Figure 3. Single-pulse ablated Sapphire (Al_2O_3) c-plane (Figure 2) after HTA at $1500\text{ }^\circ\text{C}$ for 4 h in N_2 flow at different magnifications. Focusing of $1030\text{ nm}/230\text{ fs}$ pulses was carried out with an objective lens of numerical aperture $NA = 0.14$ (Mitutoyo). Linear polarisation of the E-field of laser pulses is shown by arrow marker. Pulse energy was $E_p = 6.25\text{ }\mu\text{J}$ (on sample). Fluence was $F_p = 9.87\text{ J}/\text{cm}^2$.

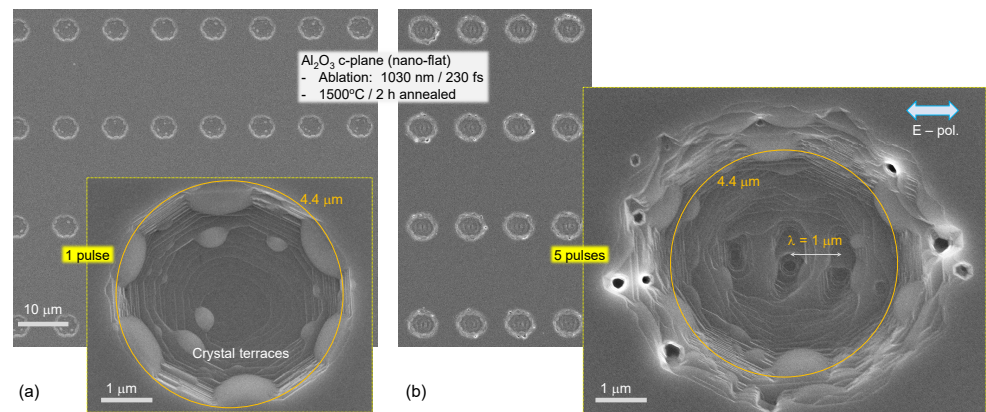


Figure 4. Sapphire (Al_2O_3) c-plane after fs-laser ablation and high-temperature annealing (HTA) at $1500\text{ }^\circ\text{C}$ for 2 h in O_2 flow. Ablation was made by: (a) one pulse and (b) five pulses per ablation site. Focusing of $1030\text{ nm}/230\text{ fs}$ pulses was carried out with an objective lens of numerical aperture $NA = 0.26$ (Mitutoyo). Linear polarisation of the E-field of laser pulses was horizontal; shown by marker. Pulse energy was $E_p = 10\text{ }\mu\text{J}$ (on sample). Fluence was $F_p = 54.5\text{ J}/\text{cm}^2$.

Figure 4 shows scanning electron microscopy (SEM) images of single and five-pulse ablated sites after HTA in O_2 flow. A single pulse of $E_p = 11.25\text{ }\mu\text{J}$ which corresponds to a fluence of $F_p = 61.32\text{ J}/\text{cm}^2$ and an average intensity of $I_p = 266\text{ TW}/\text{cm}^2$ ablated a hole of 300 nm depth and a re-healed area of $4.4\text{ }\mu\text{m}$ diameter, which almost perfectly matches the focal diameter of $4.8\text{ }\mu\text{m}$. After annealing, a perfectly smooth surface was observed near the rim of the ablated pit. When the number of pulses was two or more, formation of ripples [38] was observed (see structure of period $\Lambda \approx 1\text{ }\mu\text{m}$ at the bottom (Figure 4b)). Recovering a smooth surface during HTA in O_2 flow is a promising outcome for opto-electronic applications of 2D materials.

3.3. HTA Treatment of Back-Side Ablated Al_2O_3

Since front-surface ablation caused extensive deposition of debris, a back-side ablation was used to mitigate this issue. No liquid immersion was used as in a previous study [13]. Ablation by circular scan started from the largest diameter and was closing towards the center in concentric circles following trajectory ablating an aspherical micro-lens of $125\text{ }\mu\text{m}$ radius. After all-layer ablation, the depth of focus was changed and the next layer (into the sample from the back-side) was ablated. This protocol was robust against formation of debris and free from defects such as random non-ablated regions. The results are shown in Figure 5. Bruker ContourGT Optical Profiler was used to map surface geometry

and surface roughness. The ablation steps according to the protocol of focal position are clearly discernable together with the roughness. The height step of $\Delta z = 0.8 \mu\text{m}$ was used for most reliable ablation of aspheric dome; the step inside Al_2O_3 becomes $n \times \Delta z$ due to refractive index $n \approx 1.7$ at the wavelength of laser printing. The fluence per pulse $F_p = 4.7 \text{ J/cm}^2$ was approximately twice the threshold of sapphire ablation for the focal spot of $r = 0.61\lambda/NA = 1.4 \mu\text{m}$ radius. Up to $1 \mu\text{m}$ roughness (min-max) was observed on as ablated surfaces after ultrasonic washing. Samples were Cr-coated for SEM observation which corroborated reduction of roughness after HTA. Approximately five-times reduction of surface roughness down to $\sim 200 \text{ nm}$ was observed for the laser ablation at $NA = 0.45$ focusing. Fabrication of the micro-lens shown in Figure 5 took $\sim 15 \text{ min}$ at laser repetition rate of 200 kHz and linear scan speed of $\sim 15 \text{ mm/s}$ (pulse-to-pulse overlap was $\Delta x = 1.3 \mu\text{m}$ as well as the line-to-line separation and was comparable with the radius r of the focal spot). The designed aspherical lens has a height profile:

$$Z(s) = \frac{Cs^2}{1 + \sqrt{1 - 1(1+k)C^2s^2}} + A_4s^4 + A_6s^6 + A_8s^8 + A_{10}s^{10}, \quad (2)$$

where the coefficients $C = 1/0.15$, $k = 0$, $A_4 = 0.0093$, $A_6 = -0.005$, $A_8 = -0.0056$, $A_{10} = 0.0005$, and s is the radial distance from the optical axis.

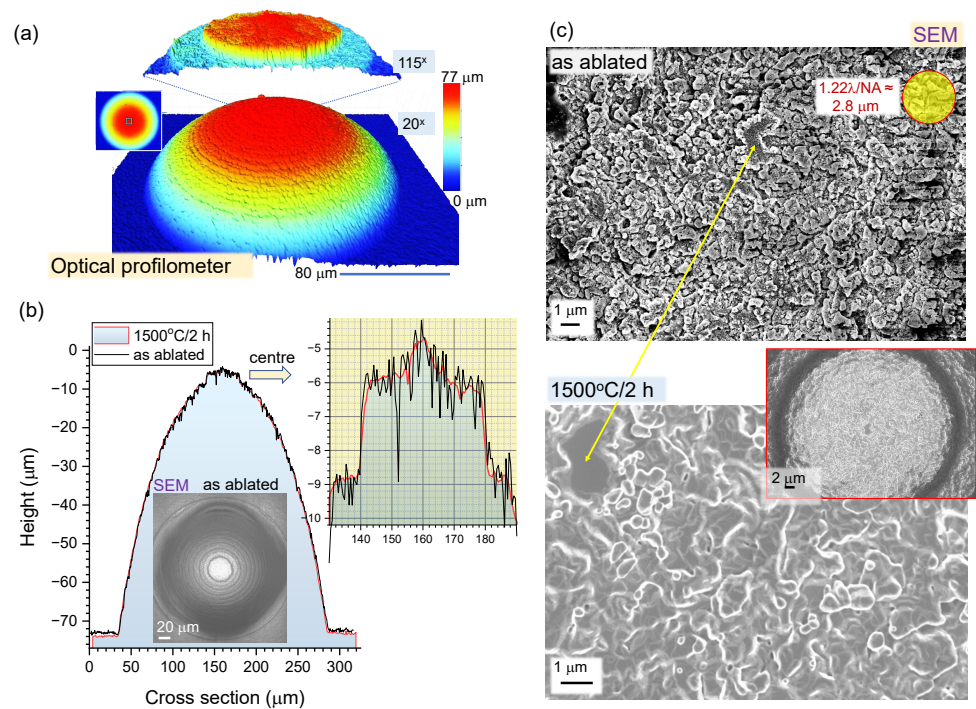


Figure 5. Back-side ablation of Al_2O_3 and HTA. (a) Optical Profiler surface map (Bruker ContourGT Optical Profiler). (b) Cross-sectional trace of surface of micro-lens before and after HTA. SEM image inset shows top-view of the lens. Top-of-lens cross-section profile is shown in the inset. (c) SEM images of the top-central region of the lens before and after HTA. Laser fabrication conditions: pulse energy $E_p = 0.29 \mu\text{J}$ ($F_p = 4.7 \text{ J/cm}^2$, $I_p = 20.5 \text{ TW/cm}^2$), pulse-to-pulse separation along scan $1.3 \mu\text{m}$ (3 pulses per irradiation site), line-to-line separation (in plane) was also 1.3 nm and along the height direction $0.8 \mu\text{m}$, wavelength $\lambda = 1030 \text{ nm}$, focusing $NA = 0.45$ (Olympus, $20\times$), repetition rate 0.2 MHz . Circularly polarised beam was set onto sample by fine tuning of $\lambda/2$ -plate in front of $\lambda/4$ -plate used as a circular polariser.

HTA made the surface smoother and the steps in z-direction less steep. HTA is responsible for the evolution of the overall aspheric shape becoming closer to the designed shape. There was almost no change in the base diameter and height of the lens (Figure 5a,b). Ablation at a fluence only twice that of the ablation threshold of the crystalline host material

contributed to a good definition of the shape of the micro-lens. In glasses, melting and surface tension-induced reshaping is taking place even without HTA [39].

The main cause of the reduction in roughness was surface restructuring during the HTA process, as illustrated in Figure 6. Sublimation could be contributing to the discernible difference in the height change of the optical profiles (Figure 5). The steps along the ablation scans become less steep. This study shows that smoother surfaces of crystalline lenses can be achieved using HTA in O₂. Smaller height steps will be tested to achieve tens-of-nm surface roughness required for optical applications.

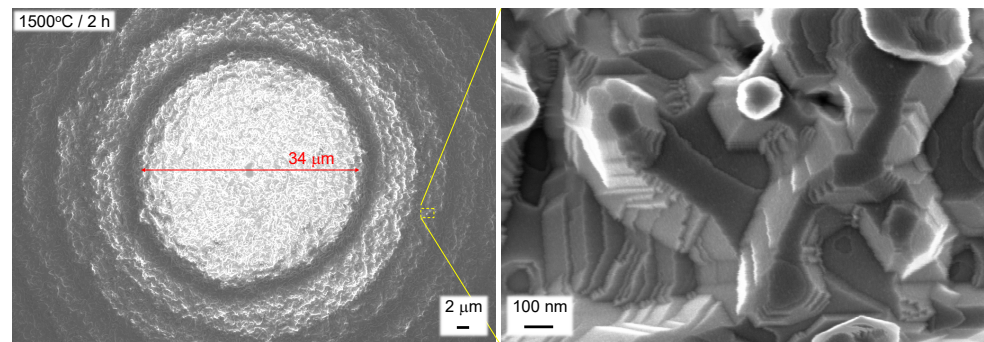


Figure 6. SEM imaging. Nanoscale reconstruction of the c-plane crystalline Al₂O₃ surface after HTA; central part of the lens.

4. Conclusions and Outlook

Sapphire ablation with different numerical apertures ($NA = 0.26$ and 0.14) and similar pulse energies ($10 \mu\text{J}$ and $6.25 \mu\text{J}$) are compared. SEM images showed the formation of ripples with period close to the wavelength of the laser irradiation for the $NA = 0.26$ and interestingly, it was half of the wavelength of the laser PHAROS (Light Conversion Ltd.) for $NA = 0.14$. After the samples had undergone high-temperature annealing at $1500 \text{ }^\circ\text{C}$ for 2 to 4 h in either an O₂ or N₂ environment, these ripples underwent restructuring and crystalline step-like structures become apparent. It was also shown that annealing in an O₂ environment reduced the amount of debris and the surface became smooth. In the case of HTA in N₂, however, pieces of debris were still present and their coarsening took place. Detailed X-ray Photoelectron Spectroscopy (XPS) experiments are planned for detailed understanding of material modification on the surface during HTA in O₂ and N₂ flow. Apparently, the O₂ flow was an important factor for restoration of a smooth c-plane surface by HTA.

We show that the restructuring of laser-ablated crystalline surfaces can be applied to the fabrication of micro-optical elements in reducing the surface roughness and allowing for tighter control over the surface profile while maintaining the precision of a shape definition. This is different from glasses [40], where HTA causes a surface tension-driven reflow and formation of spherical surfaces which might be different from the required shape for a defined optical function. Back-side ablation in air was used to define an aspherical micro-lens profile, which was not altered by HTA while surface roughness was markedly reduced. The true extent of the control over surface roughness is yet to be fully explored using this technique. The optimal time of annealing and the optimal temperature to achieve the most restructuring without sacrificing the surface profile will be determined in future studies. Sublimation via solid-to-gas occurring along with solid-fusion-vaporisation stages during HTA needs better understanding and can be different in other crystals.

Author Contributions: Conceptualisation, S.J. and S.H.N.; investigation, D.S., A.T., D.M. and T.K.; writing—original draft preparation, S.J. and D.S.; review and editing, all authors. All authors have read and agreed to the published version of the manuscript.

Funding: This research was funded by the Australian Research Council, grant number LP190100505. S.J. is grateful for startup funding from the Nanotechnology Facility at Swinburne and to the Workshop-on-Photonics for the technology transfer project, which installed the first industrial-grade microfabrication setup in Australia. Part of this study was made during a Grand Challenge undergraduate project of A.T. Mechanisms of light-matter interactions were discussed with Prof. Eugene G. Gamaly. We are grateful to Laser Systems Ltd., Sapporo, Japan and Tecdia Ltd., Tokyo, Japan companies for providing ultra-thin 30 μm -thick Al_2O_3 samples.

Institutional Review Board Statement: Not applicable.

Informed Consent Statement: Not applicable.

Data Availability Statement: The data presented in this study are available on request from the corresponding author.

Conflicts of Interest: The authors declare no conflict of interest.

Appendix A. HTA of Al_2O_3 in N_2

The Al_2O_3 HTA in O_2 flow caused restructuring of surface at the ablated regions and sublimation of debris (Figure 5) contrasting the surface annealed in N_2 flow (Figure A1). The phase diagrams single out ALN and ALON [32] for surface modification shown in Figure A1.

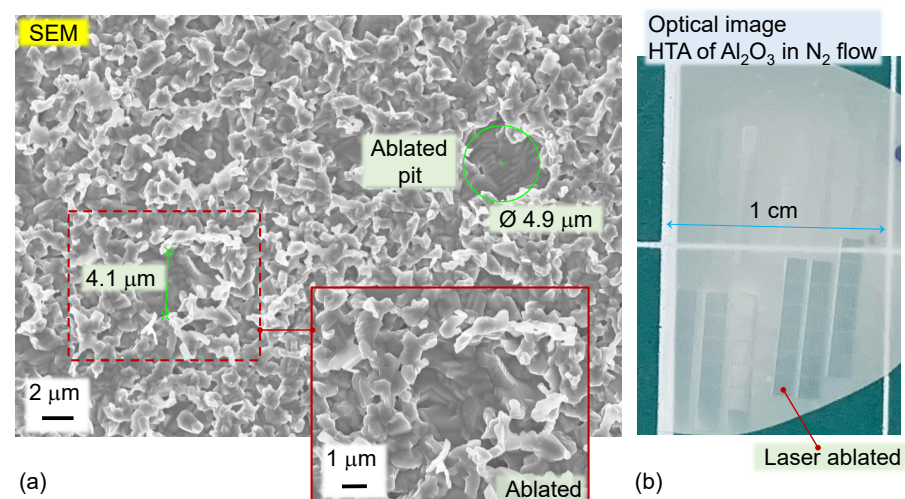


Figure A1. (a) SEM images of ALON nanotextured surfaces around the ablated regions. (b) The ablated areas becomes translucent (Al_2O_3 was placed on a green-colored pad for photo). Ablation was carried out at similar conditions to those shown in Figure 4. Thickness of Al_2O_3 was $\sim 30 \mu\text{m}$; initially, it was two-side polished to a high optical transparency.

References

- Batani, K.; Batani, D.; He, X.; Shigemori, K. Recent progress in matter in extreme states created by laser. *Matter Radiat. Extrem.* **2022**, *7*, 013001. [[CrossRef](#)]
- Juodkazis, S.; Nishimura, K.; Tanaka, S.; Misawa, H.; Gamaly, E.E.; Luther-Davies, B.; Hallo, L.; Nicolai, P.; Tikhonchuk, V. Laser-Induced Microexplosion Confined in the Bulk of a Sapphire Crystal: Evidence of Multimegabar Pressures. *Phys. Rev. Lett.* **2006**, *96*, 166101. [[CrossRef](#)] [[PubMed](#)]
- Vailionis, A.; Gamaly, E.G.; Mizeikis, V.; Yang, W.; Rode, A.; Juodkazis, S. Evidence of super-dense Aluminum synthesized by ultra-fast micro-explosion. *Nat. Commun.* **2011**, *2*, 445. [[CrossRef](#)] [[PubMed](#)]
- Zelovich, Y.B.; Raizer, Y.P. *Physics of Shock Waves and High-Temperature Hydrodynamic Phenomena*; Dover, Dover Books on Physics: New York, NY, USA, 2002.
- Campanella, B.; Legnaioli, S.; Pagnotta, S.; Poggialini, F.; Palleschi, V. Shock waves in laser-induced plasmas. *Atoms* **2019**, *7*, 57. [[CrossRef](#)]
- Juodkazis, S.; Nishimura, K.; Misawa, H.; Ebisui, T.; Waki, R.; Matsuo, S.; Okada, T. Control over the State of Crystallinity: Sapphire. *Adv. Mat.* **2006**, *18*, 1361–1364. [[CrossRef](#)]

7. Huang, H.H.; Juodkakis, S.; Gamaly, E.; Nagashima, T.; Yonezawa, T.; Hatanaka, K. Spatio-temporal control of THz emission. *Commun. Phys.* **2022**, *5*, 134. [[CrossRef](#)]
8. Juodkakis, S.; Misawa, H.; Gamaly, E.G.; Luther-Davis, B.; Hallo, L.; Nicolai, P.; Tikhonchuk, V. Is the nano-explosion really microscopic? *J. Non-Crystall. Solids* **2009**, *355*, 1160–1162. [[CrossRef](#)]
9. Nath, G. Approximate analytical solution for the propagation of shock waves in self-gravitating perfect gas via power series method: isothermal flow. *J. Astrophys. Astron.* **2020**, *41*, 21. [[CrossRef](#)]
10. Sharova, Y.S.; Glazyrin, S.I.; Gasilov, V.A. Study of the Influence of the Background Neutral Component on the Dynamics of the Envelope in Supernova Remnants. *Astron. Lett.* **2021**, *47*, 746–753. [[CrossRef](#)]
11. Petruk, O.; Kuzyo, T.; Orlando, S.; Pohl, M.; Brose, R. Magneto-hydrodynamic simulations of young supernova remnants and their energy-conversion phase. *Mon. Not. R. Astron. Soc.* **2021**, *505*, 755–770. Available online: <https://academic.oup.com/mnras/article-pdf/505/1/755/39549986/stab1319.pdf> (accessed on 1 May 2023). [[CrossRef](#)]
12. Hirashima, K.; Moriwaki, K.; Fujii, M.; Hirai, Y.; Saitoh, T.; Makino, J. Predicting the Expansion of Supernova Shells Using Deep Learning toward Highly Resolved Galaxy Simulations. *Proc. Int. Astron. Union* **2020**, *16*, 209–214. [[CrossRef](#)]
13. Hua, J.G.; Liang, S.Y.; Chen, Q.D.; Juodkakis, S.; Sun, H.B. Free-Form Micro-Optics Out of Crystals: Femtosecond Laser 3D Sculpturing. *Adv. Func. Mat.* **2022**, *32*, 2200255. [[CrossRef](#)]
14. Marupalli, B.C.; Adhikary, T.; Sahu, B.; Mitra, R.; Aich, S. Effect of annealing temperature on microstructure and mechanical response of sputter deposited Ti-Zr-Mo high temperature shape memory alloy thin films. *Appl. Surf. Sci. Adv.* **2021**, *6*, 100137. [[CrossRef](#)]
15. Shklyaev, A.; Latyshev, A. Surface Morphology Transformation Under High-Temperature Annealing of Ge Layers Deposited on Si(100). *Nanoscale Res. Lett.* **2016**, *11*, 366. . [[CrossRef](#)] [[PubMed](#)]
16. Woo, S.; Jeong, H.; Lee, S.; Seo, H.; Lacotte, M.; David, A.; Kim, H.; Prellier, W.; Kim, Y.; Choi, W.S. Surface properties of atomically flat poly-crystalline SrTiO₃. *Sci. Rep.* **2015**, *5*, 8822. [[CrossRef](#)]
17. Gailevicius, D.; Padolskyte, V.; Mikoliunaite, L.; Sakirzanovas, S.; Juodkakis, S.; Malinauskas, M. Additive-manufacturing of 3D glass-ceramics down to nanoscale resolution. *Nanoscale Horiz.* **2019**, *4*, 647–651. [[CrossRef](#)]
18. Acosta-Alba Pablo, E.; Kononchuk, O.; Gourdel, C.; Claverie, A. Surface self-diffusion of silicon during high temperature annealing. *J. Appl. Phys.* **2014**, *115*, 134903. [[CrossRef](#)]
19. Liu, M.; Zhou, H.; Zhu, H.; Yue, Z.; Zhao, J. Microstructure and dielectric properties of glass/Al₂O₃ composites with various low softening point borosilicate glasses. *J. Mater. Sci. Mater. Electron.* **2012**, *23*. [[CrossRef](#)]
20. Uwaha, M.; Saito, Y. Kinetic smoothing and roughening of a step with surface diffusion. *Phys. Rev. Lett.* **1992**, *68*, 224–227. . [[CrossRef](#)]
21. Zaluska-Kotur, M.A.; Krzyzewski, F.; Krukowski, S.; Czernecki, R.; Leszczynski, M. Structures Built by Steps Motion during Sublimation from Annealed GaN(0001) Surface. *Cryst. Growth Des.* **2013**, *13*, 1006–1013. [[CrossRef](#)]
22. Kazantsev, D.; Akhundov, I.; Rudaya, N.; Kozhukhov, A.; Alperovich, V.; Latyshev, A. Thermal roughening of GaAs surface by unwinding dislocation-induced spiral atomic steps during sublimation. *Appl. Surf. Sci.* **2020**, *529*, 147090. [[CrossRef](#)]
23. Kazantsev, D.; Akhundov, I.; Karpov, A.; Shwartz, N.; Alperovich, V.; Terekhov, A.; Latyshev, A. Monte Carlo simulation of GaAs(001) surface smoothing in equilibrium conditions. *Appl. Surf. Sci.* **2015**, *333*, 141–146. [[CrossRef](#)]
24. Mundschau, M.; Bauer, E.; Telieps, W.; Swiehn, W. Atomic steps on Si100 and step dynamics during sublimation studied by low-energy electron microscopy. *Surf. Sci.* **1989**, *223*, 413–423. [[CrossRef](#)]
25. Sheglov, D.V.; Sitnikov, S.V.; Fedina, L.I.; Rogilo, D.I.; Kozhukhov, A.S.; Latyshev, A.V. From Self-Organization of Monoatomic Steps on the Silicon Surface to Subnanometer Metrology. *Optoelectron. Instrum. Data Process.* **2020**, *56*, 533–544. [[CrossRef](#)]
26. Readey, D.; Kuczynski, G. Sublimation of Aluminum Oxide in Hydrogen. *J. Am. Ceram. Soc.* **2006**, *49*, 26–29. [[CrossRef](#)]
27. Andre, P.; Abbaoui, M.; Augeard, A.; Desprez, P.; Singo, T. Study of Condensed Phases, of Vaporization Temperatures of Aluminum Oxide and Aluminum, of Sublimation Temperature of Aluminum Nitride and Composition in an Air Aluminum Plasma. *Plasma Chem. Plasma Process.* **2016**, *36*, 1161–1175. [[CrossRef](#)]
28. Gamaly, E.E.; Juodkakis, S.; Nishimura, K.; Misawa, H.; Luther-Davies, B.; Hallo, L.; Nicolai, P.; Tikhonchuk, V. Laser-matter interaction in a bulk of a transparent solid: confined micro-explosion and void formation. *Phys. Rev. B* **2006**, *73*, 214101. [[CrossRef](#)]
29. Hua, J.G.; Ren, H.; Huang, J.; Luan, M.L.; Chen, Q.D.; Juodkakis, S.; Sun, H.B. Laser-Induced Cavitation-Assisted True 3D Nano-Sculpturing of Hard Materials. *Small* **2023**, 2207968. [[CrossRef](#)]
30. Liu, X.Q.; Zhang, Y.L.; Li, Q.K.; Zheng, J.X.; Lu, Y.M.; Juodkakis, S.; Chen, Q.D.; Sun, H.B. Biomimetic sapphire windows enabled by inside-out femtosecond laser deep-scribing. *Photonix* **2022**, *3*, 1. [[CrossRef](#)]
31. Mahesh, J.Y.; Aravindan, S.; Rao, P.V.; Yogita, M.; Singh, J.P. Surface morphology evolution of C-plane sapphire during multi-step thermal annealing. *Surf. Topogr. Metrol. Prop.* **2022**, *10*, 045015. . [[CrossRef](#)]
32. Prosvirnin, D.V.; Kolmakov, A.G.; Larionov, M.D.; Prutskov, M.E.; Alikhanyan, A.S.; Samokhin, A.V.; Lysenkov, A.S.; Titov, D.D. Effect of sintering methods and temperatures on porosity of the ceramics from aluminum oxinitride. *IOP Conf. Ser. Mater. Sci. Eng.* **2018**, *347*, 012030. [[CrossRef](#)]
33. Kudrius, T.; Šlekys, G.; Juodkakis, S. Surface-texturing of sapphire by femtosecond laser pulses for photonic applications. *J. Phys. D: Appl. Phys.* **2010**, *43*, 145501. [[CrossRef](#)]
34. Buividas, R.; Aharonovich, I.; Seniutinas, G.; Wang, X.W.; Rapp, L.; Rode, A.V.; Juodkakis, S. Photoluminescence from voids created by femtosecond-laser pulses inside cubic-BN. *Opt. Lett.* **2015**, *40*, 5711–5713. [[CrossRef](#)] [[PubMed](#)]

35. Hsu, W.H.; Masim, F.; Balcytis, A.; Juodkazis, S.; Hatanaka, K. Dynamic position shifts of X-ray emission from a water film induced by a pair of time-delayed femtosecond laser pulses. *Opt. Express* **2017**, *25*, 24109–24118. [[CrossRef](#)]
36. Gamaly, E.G.; Rode, A.V. Ultrafast re-structuring of the electronic landscape of transparent dielectrics: New material states (Die-Met). *Appl. Phys. A* **2018**, *124*, 278. [[CrossRef](#)]
37. Ng, S.; Juodkazis, S. *Nanoscale Plasmonic Printing in Ultrafast Laser Nanostructuring: The Pursuit of Extreme Scales*; Stoian, R., Bonse, J., Eds.; Springer Series in Optical Science; Springer: Berlin/Heidelberg, Germany, 2023; Volume 239, Chapter 25.
38. Buividas, R.; Mikutis, M.; Juodkazis, S. Surface and bulk structuring of materials by ripples with long and short laser pulses: Recent advances. *Prog. Quantum Electron.* **2019**, *38*, 119–156. [[CrossRef](#)]
39. Vanagas, E.; Kudryashov, I.; Tuzhilin, D.; Juodkazis, S.; Matsuo, S.; Misawa, H. Surface nanostructuring of borosilicate glass by femtosecond nJ energy pulses. *Appl. Phys. Lett.* **2003**, *82*, 2901–2903. [[CrossRef](#)]
40. Bach, H.; Krause, D. Technical Glasses—Physical and Technical Properties. In *Technical Report*; SCHOTT AG: Mainz, Germany, 2020.

Disclaimer/Publisher’s Note: The statements, opinions and data contained in all publications are solely those of the individual author(s) and contributor(s) and not of MDPI and/or the editor(s). MDPI and/or the editor(s) disclaim responsibility for any injury to people or property resulting from any ideas, methods, instructions or products referred to in the content.